Bio-Inspired Synthesis of High-Performance Nanocomposite Catalysts for Hydrogen Oxidation

*Chang Sun Kong, Hong-Li Zhang, Ferenc Somodi, and Daniel E. Morse**

A biologically inspired synthesis method is presented as a new tool for the design of novel electrochemically active materials, focusing on the advantages for fuel cell development. The need for cost-effective, high-performance materials is driving contemporary fuel cell research, with the expectation that advances in synthetic methods will be necessary for commercialization of this energy technology. Highly active electrocatalysts for proton-exchange-membrane (PEM) fuel cells are being developed, by combining a kinetically controlled synthesis method of the nanocrystalline metal catalyst with the mesoscale assembly of two morphologically different carbon building blocks of the supporting matrix. These methods provide access to new combinations of porosity, conductivity and electrochemical hydrogen oxidation. The relationships between the porous morphologies of the carbon matrices, the sizes of the platinum nanocrystals and their resulting electrochemical activities are discussed, correlating these with the relevant fuel cell principles.

1. Introduction

For the past several decades, proton-exchange-membrane (PEM) fuel cells have been considered promising energy devices with potentially wide applications in portable, transportation and stationary power systems. Although wide scale commercialization has not yet been established, the advantages of the PEM fuel cell as a replacement for the internal combustion engine, with its low emissions, quiet operation, high energy conversion efficiency, adaptability for use with hydrogen (as well as a wide range of gaseous and liquid fuels) drive continued research and development. The principal obstacles to adoption of fuel-cell technology remain cost and insufficient durability.

Dr. C. S. Kong, Dr. H.-L. Zhang, Dr. F. Somodi
Institute for Collaborative Biotechnologies
California NanoSystems Institute
and Materials Research Laboratory
University of California
Santa Barbara, CA 93106, USA
Prof. D. E. Morse
Institute for Collaborative Biotechnologies
California NanoSystems Institute
Materials Research Laboratory
and Department of Molecular
Cellular, and Developmental Biology
University of California
Santa Barbara, CA 93106, USA
E-mail: d_morse@lifesci.ucsb.edu

DOI: 10.1002/adfm.201203882

Biological systems have evolved adaptations that can offer innovative paths to solutions for problems in human technology. As we describe below, our aim is utilize the principle of kinetically controlled nanofabrication, inspired by discoveries of the mechanisms underlying the biological synthesis of the mineral skeleton of a marine sponge[1–3] to control the growth of high-performance nanocrystals of platinum (Pt) for use as the fuel-oxidizing catalyst in PEM fuel cell devices. This biologically inspired synthesis route is combined with a new mesoscale assembly of a carbon-carbon composite that serves as the support for the growth of the nanocrystalline Pt. Tunability of the morphological properties of the carbon matrix and its resulting nanocomposite with Pt offers advantages for its mutifunctional use as electrodes for PEM fuel cells. We have investigated the relationships between the hierarchical porous structures of the carbon composites, the size and structure of the Pt nanocrystals and electrolyte ionomers, and the electrochemical activity of the nanocomposite carbon-Pt catalysts, correlating those with the principles of fuel cell reactions.

2. Principles of PEM Fuel Cell Design

A typical PEM fuel cell electrode membrane-electrode assembly (MEA) contains an anode and cathode separated by a polymer electrolyte membrane.[4] Each electrode consists of a porous thin film of a polymeric electrolyte containing nanoparticles of a metal catalyst and a conductive carbon matrix. During fuel cell operation, reactant gases (e.g., hydrogen and oxygen) are supplied to the MEA through the anode and cathode, respectively, while the electrons produced by oxidation of the hydrogen are removed via a current between the two electrodes. Since the reactants and products of fuel cell reactions must be transported simultaneously into and out of the porous structure of the electrodes, synthesis of a MEA structure capable of supporting the efficient diffusion of multiple phases (gases, liquids, electrons, and protons) is an essential target for the design of fuel cell electrodes. Optimization of the size, distribution and orientation of pores in the electrodes is needed to achieve both the large reactive surface area required for efficient catalysis and the efficient transport of the gaseous reactants and water by-product. Cost effectiveness requires the lowest loading of expensive metal (e.g., Pt) while maximizing

exposure of its electrochemically active surface area and optimizing contact between the nanocrystalline metal, reactant gas, electrolyte ionomer and carbon matrix.[5]

2.1. Carbon Supported Platinum Catalysts

A typical electrode structure of a PEM fuel cell is made of a carbon-supported Pt catalyst layer directly deposited on the surface of a gas-diffusion layer or at the interface with a polymer electrolyte membrane, permitting a significant decrease in the amount of Pt required. By dispersing nano-size Pt particles in a porous carbon matrix, the efficiency of the Pt catalyst is maximized as a result of the large surface-area-to-volume ratio.[6–8]

Various carbon polymorphs[9–13] have been extensively explored as the conductive matrices of PEM fuel cell catalysts to offer both high electrical conductivity and high porosity. The carbon support material chosen for the formation of a catalyst layer becomes the structural and reactive component in a fuel cell system; additionally, as in the work reported here, it may also play a key role as the substrate for nucleation and growth of the Pt nanocrystals.

2.2. Triple-Phase Boundary: The Effect of Pore Structure of Carbon-Support Materials

Carbon-based porous electrodes in a PEM fuel cell provide the pathways for the supply of reactants (fuel and oxidant) and the extraction of products (electrons, protons, vapor or liquid phase water, etc.) while additionally providing the catalytically and electrochemically active sites for the conversion of chemical energy to electricity. These active sites are referred to as the triple-phase boundary (TPB) sites, where oxidant, reductant and catalyst simultaneously interact. When the Pt nanocrystals are grown within the carbon matrix, the size of the resulting Pt nanocrystals is determined both by the geometry and accessibility of the pores of the matrix, and by surface interactions, reactant fluxes, temperature, and other factors governing the relative rates of nucleation and growth. Optimal geometry of pores in the carbon matrix must allow ready access of reactant gases, with connectivity to the molecular network of electrolyte ionomers providing transport of protons to the electrolyte membrane. In the widely used Nafion electrolyte membrane, aggregates of perfluorosulfonate form ionomeric clusters 30–50 nm in diameter; pores in the carbon matrix larger than this diameter are thus required for ready access of the electrolyte.[14] For this reason, Pt particles located in smaller pores may not be effectively contacted by the electrolyte, thereby reducing the effectively available active area of the catalyst.[15–18] On the other hand, Pt sites completely covered by electrolyte clusters may be shielded from access to the reactants.

Considering only the Pt nanocrystals themselves, smaller Pt nanoparticles might be expected to have higher specific electrochemical (i.e., catalytic) activity in proportion to their higher specific surface area. However, the factors discussed immediately above militate against this expectation. In fact, experimental results have shown that as Pt size is decreased below some optimum, both fuel cell performance and long-term durability are decreased.[19–22] Thus, the optimal Pt particle size needed to achieve highest electrochemical performance is dependent in a complex manner on the size, distribution and orientation of pores in the carbon matrix and with the correlated accessibility of reactant gases and connectivity with electrolyte networks.

3. Bio-Inspired Growth of Platinum Nanocrystals in Carbon Matrices

Biological systems of mineral synthesis are recognized as paragons of complex multifunctional architectural control. Their structures are achieved through unique, energy-efficient chemical mechanisms and materials building processes that have been shaped through millenia of evolution and natural selection, and offer advantages over present anthropogenic approaches.[23,24] Translating the underlying mechanisms we discovered governing the catalytic nanofabrication of silica to form the skeletal elements of a marine sponge, we developed a generic, kinetically controlled catalytic method for the synthesis of a large number of nanocrystalline metals and metal oxides, hydroxides, phosphates, nitrides and sulfides.[25–29] We show here that this method can be adapted to grow nanocrystals of Pt in high uniformity on the surfaces and throughout the internal pore structures of a variety of carbon matrices.

4. Carbon-Carbon Composites as Platinum Catalyst Support Matrices

Carbon-carbon composites typically are used for electronic applications in which thermal and mechanical stability are required.[30] Recent reports describe the use of carbon-carbon composites as Pt support matrices.[31–34] However, these used only simple mixtures, or those that sintered at relatively low temperatures (250–350 °C), of different kinds of carbon materials, such as reduced graphene oxide (RGO) and carbon black,[31] two carbon blacks with different morphologies,[32] carbon black and carbon nanotubes (CNTs),[33] and graphene and CNTs.[34] Because CNTs can provide high electrical conductivity, they have been used in fuel cell materials to increase reactivity. However, it was found that chemical functionalization of the CNT surface which results in structural damages decreases its electrical conductivity.[35] In this work, instead of functionalizing CNTs for the enhancement of surface properties to enhance Pt binding, we have used multiwall CNTs to improve electrical conductivity and corrosion stability by combining them with carbon black aggregates. The aggregates of highly porous carbon black particles are interconnected by CNTs, extending long-distance conductivity while retaining the high porosity of the carbon matrix.

5. Methods

5.1. Preparation of Carbon-Carbon Composite-Supported Pt Catalysts

Carbon-carbon composites were synthesized using carbon black (Vulcan XC-72, Cabot Co.) and multi-walled CNT powders

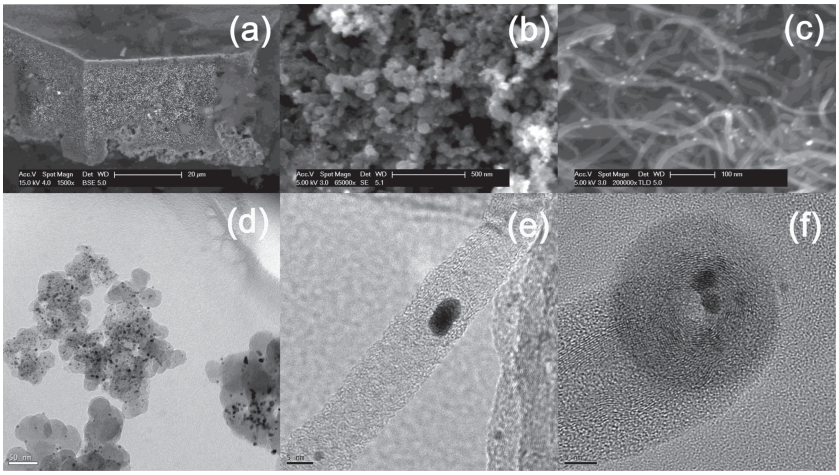

Figure 1. a) Backscattered scanning electron microscope (SEM), b) SEM, and d) transmission electron microscope (TEM) images of carbon black (Vulcan XC-72)-supported Pt catalyst nanocrystals; c) SEM and e,f) TEM images of carbon nanotube (CNT)-supported Pt catalyst nanocrystals grown on the surface of a nanotube wall (e) and a pore mouth (f); scale bar in (d) = 50 nm and (e,f) = 5 nm, respectively.

(Baytube, C150HP, Bayer MaterialScience). After the two carbon nanoforms were mixed in various compositional ratios in deionized water, the solution was ultrasonicated for 1 h to obtain a well dispersed suspension. The suspension was then dried in the mineral oil bath at 90 °C in air and the dried cake of carbon mixture was heat-treated in a tube furnace at 1100 °C for 2 h (with two different ramping rates, i.e., 2 °C/min (slow) and 10 °C/min (fast)) while purging the samples with nitrogen gas (10 mL/min).

Carbon-supported Pt catalysts (15 wt% Pt) were synthesized from aqueous solutions of platinum (IV) chloride ($PtCl_4$, Sigma-Aldrich) that had first been allowed to infiltrate suspensions of various carbon support materials (carbon black, CNTs, and carbon composites) under the diffusion of ammonia (NH_3) vapor at room temperature. To obtain Pt@carbon catalysts with 15 wt% of Pt content, carbon powders (0.1 g) were added to an aqueous solution of $PtCl_4$ (40 mL, 2 mM). After ultrasonic stirring for 30 min, the suspension was transferred to a glass flask connected to a second flask containing an aqueous solution of NH_4OH (2 wt%). NH_3 vapor was allowed to diffuse at room temperature into the mixed suspension for 24 h, during which it formed an adduct with the $PtCl_4$. This intermediate was collected by filtration and dried at 90 °C in an oil bath. Thermal decomposition under N_2/H_2 (95%/5%) initiated nucleation and growth of the Pt nanocrystals in a furnace at a temperature of 500 °C for 30 min. The ramping rate from room temperature to thermal treatment temperature was 10 °C/min.

5.2. Physicochemical and Electrochemical Characterizations

Pt nanocrystals embedded in carbon matrices were examined by X-ray diffraction (XRD) (X'PERT powder diffractometer (Cu Kα radiation)). The Cu Kα tube was operated at 45 kV and a current of 40 mA. The average size of Pt particles, d (in Å), was estimated from the half-width of the Pt(111) diffraction peak using the Scherrer equation.[36]

$$d = \frac{k\lambda}{B\cos\theta} \quad (1)$$

Here, k is a shape factor which is referred to as Scherrer constant (k = 0.9), λ is the X-ray wavelength (Cu Kα = 1.54 Å), B is the diffraction peak width in radians, i.e. the peak broadening at the full width at half-maximum (FWHM), and θ is the angle at the maximum intensity.

Morphologies of the carbon matrices and the Pt@carbon composites were examined by scanning electron microscopy (SEM) using a FEI XL40 Sirion FEG Digital Electron Scanning Microscope and by transmission electron microscopy (TEM) using a FEI Tecnai G^2 Sphera Microscope. Samples were suspended in isopropyl alcohol for deposition on the EM grids.

BET surface areas of the carbons were measured with nitrogen adsorption at the boiling point of 77 K using a BET porosimeter (TriStar, Micromeritics). From the model developed by Brunauer, Emmet, and Teller in 1940s, the specific surface area of the porous carbons was determined. Pore size distributions were calculated by the Barrett-Joyner-Halenda (BJH) method from N_2 adsorption data in terms of the incremental pore volume.

Cyclic voltammetry measurements were carried out to investigate the electrochemically active area of Pt(15wt%)@carbon catalysts (CHInstruments). Pt catalysts mixed with isopropyl alcohol and Nafion ionomer solution were coated on the surface of a glassy carbon working electrode (electrode diameter = 3 mm). The voltage was swept at the rate of 10 mV/s in H_2SO_4 solution (0.5 M) at room temperature, with measurement of the current generated by the desorption of hydrogen molecules in the form of protons and electrons.

6. Results and Discussion

Figure 1 shows SEM and TEM images of Pt catalysts supported by a single carbon matrix, i.e., carbon black (Vulcan XC-72) or multi-walled CNT. Carbon black forms a network of aggregates of small spherical particles (Figure 1b). The average size of Pt nanocryatals grown on Vulcan XC-72 is approximately 3.5 nm, as calculated from the broadening of the Pt(111) XRD peak. As shown from the back-scattered electron SEM image, Figure 1a, the heavy Pt particles (seen as bright spots) are uniformly dispersed in the carbon matrix. From the SEM and TEM images of multi-walled CNT-supported Pt catalysts, it is observed that Pt nanocrystals are grown on the tube surfaces and at the pore mouths. The average size of Pt nanocrsytals measured from XRD peak broadening is approximately 4.83 nm, which is larger than the Pt nanocrystals nucleated on the carbon black matrices. According to the IUPAC (International Union of Pure and Applied Chemistry),[37] the pore sizes are classified into three different groups, i.e. micropores (<2 nm), macropores (>50 nm), and mesopores (2–50 nm). As discussed below, we

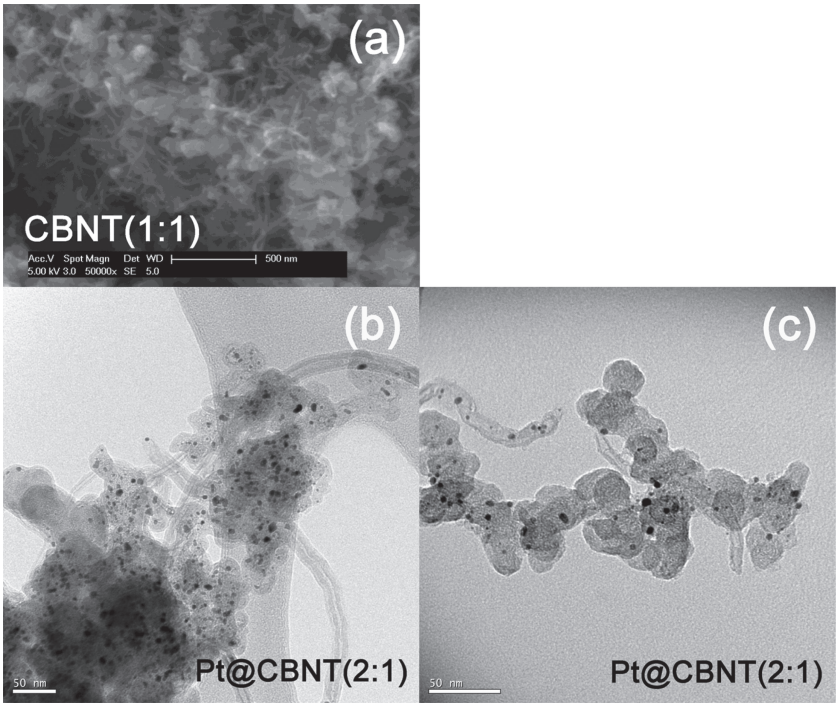

Figure 2. a) SEM image of a carbon-carbon composite (Vulcan XC-72 and multiwall CNT) and b,c) TEM images of carbon composite matrices showing dispersion of Pt nanocrystals; scale bar in (a) = 500 nm and (b,c) = 50 nm, respectively.

add a functional definition of porosity in terms of electrochemical activity.

SEM and TEM images of mesoscale assemblies of two carbon building blocks, i.e., carbon black (CB) and nanotube (NT), are shown in **Figure 2**. The morphologies of carbon matrices were tailored by compositional and thermal tuning of different carbon nanoforms. Figure 2 clearly shows that the two kinds of carbons are cross-connected each other, after heat treatment at 1100 °C, forming a homogeneous network structure. It is observed that under the processing regimes investigated here, the two different carbon blocks are linked at the mesoscale, rather than resulting from structural breakdown and rearrangement of the constituent carbon atoms. As shown in the Figure 2b,c, Pt nanocrystals of uniform size were grown in these new carbon matrices. Kinetically controlled synthesis has resulted in the uniform dispersion of the Pt nanocrystals within the carbon composite matrices.

Figure 3 and **Figure 4** show the porous morphologies of the carbon support materials analyzed by Brunauer-Emmett-Teller (BET) porosimetry. It is shown that the pore structure of the composite carbon materials can be delicately tailored by combining two types of carbon nanoforms (carbon black and nanotube) through compositional and thermal tuning. One important observation is that the relative pore area is changed in different ways at different pore size ranges. In Figure 3, for the case of CB (Vulcan XC72), the portion of the surface area corresponding to mesopores is 73.08%, while 76.91% of the pore surface area is mesoporous in the CNT marix. However, the mesopores formed in the CNT matrix are considerably larger (10–50 nm diameter) than those in the CB matrix. Reciprocally, the CB matrix has more micropores. In the range of 2–10 nm pore diameter, which is comparable to the minimal size of Pt nanocrystals that can act electrocatalytically, the pore area is increased as the amount of carbon black is increased. However, in the range of 50–100 nm pore diameter, comparable to the minimal size range accessible to the Nafion ionomers, the pore area is increased as the amount of carbon nanotube is increased. It is also found that the proportion of mesopores is increased under the high temperature ramping rate (10 °C/min), whereas total BET surface area and pore volume are slightly decreased. Thus, for the efficient transport of both reactant gases to the catalyst nanocrystals, and for the efficient transport of protons (H^+) through the electrolyte membrane, the pore size distribution must be carefully optimized.

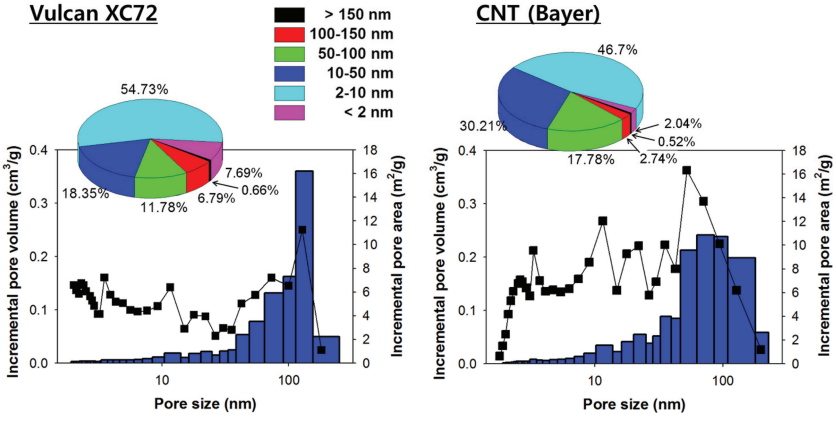

Figure 3. Pore size distribution (blue-color bar plots show incremental pore volume, and line-symbol (▪) plots show incremental pore area) of carbon black and CNTs; pie charts represent the percentage of pore areas occupied by each pore size range.

The variation of surface area of the porous carbon matrices as a function of pore size is shown in **Figure 5** in terms of the compositional ratios of carbon black (CB) and nanotube (NT). As more carbon nanotubes were added, total surface area gradually increased. In particular, the surface area in the mesopore size range (2–50 nm, blue and cyan region) increased while the surface area of micropores (<2 nm) decreased. Adding nanotubes to the matrix reduced the proportion of micropores, allowing the formation of Pt nancrystals smaller than 2 nm while not contributing to the TPB zone. Instead, the proportion of mesopores contributing to the

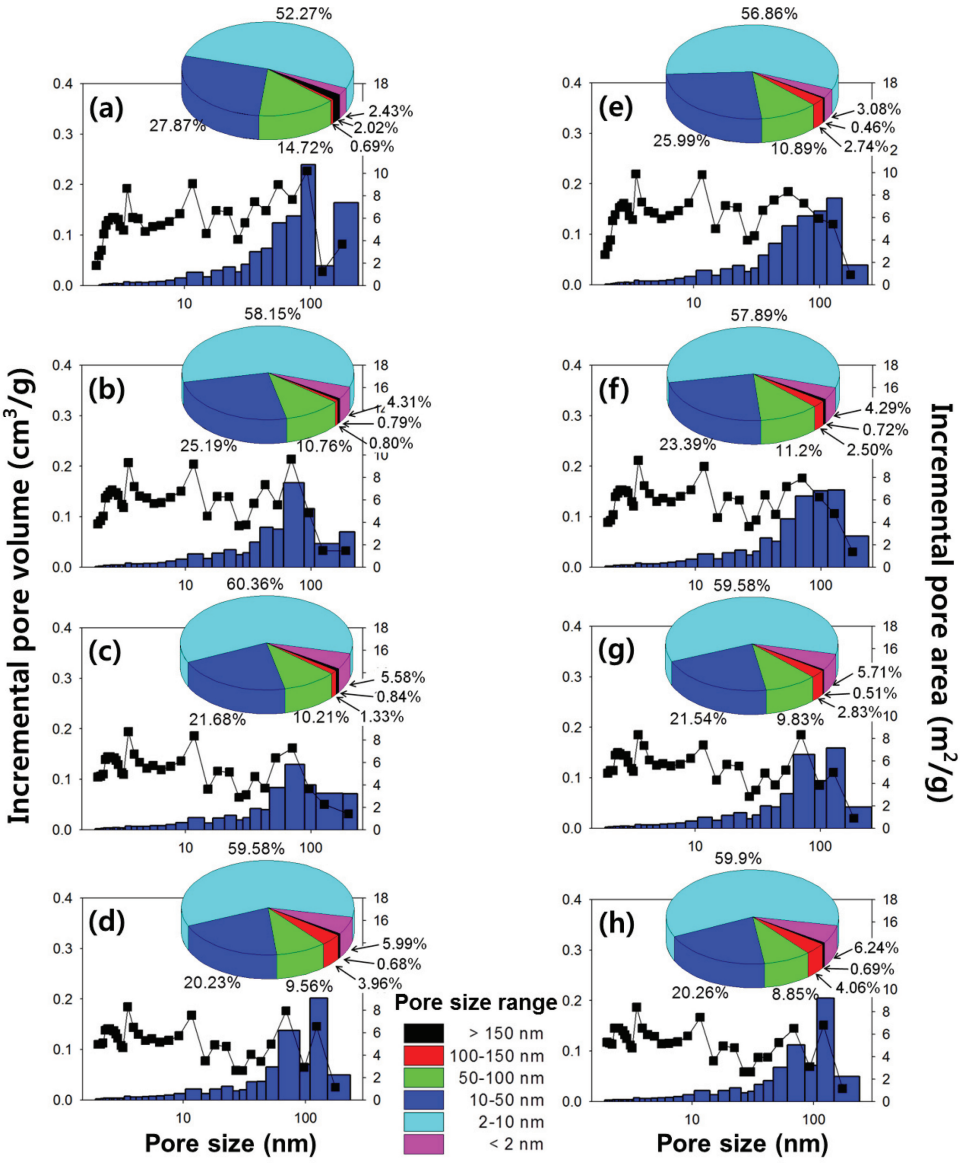

Figure 4. Pore size distribution (blue-color bar plots show incremental pore volume; linesymbol (▪) plots show incremental pore area) of carbon black-CNT composite matrices; pie charts represent the percentage of pore areas occupied by each pore size range; a) CBNT(1:2)_f; b) CBNT(1:1)_f; c) CBNT(2:1)_f; d) CBNT(3:1)_f; e) CBNT(1:2)_s; f) CBNT(1:1)_s; g) CBNT(2:1)_s; h) CBNT(3:1)_s; where, s stands for "slow" ramping rate (2 °C/min), and f stands for "fast" ramping rate (10 °C/min) of carbothermal reduction.

formation of the TPB zone was increased. Surface areas and pore structure data are tabulated in **Table 1**, obtained from BET measurements.

The influence of the surface area of the carbon matrices on Pt nanocrystal size was investigated (**Figure 6**). From the broadening of diffraction peaks depending on the size of nanocrystallites (Scherrer equation),[36] the average size of Pt crystals was calculated. The Pt(111) peak which shows the higher signal-to-noise ratio than other peaks (i.e., Pt (200), Pt(220), Pt(311), etc.) was used for these calculations (Figure 6c). A correlation between the size of Pt particles and the surface area of the carbon matrices is observed (Figure 6b). One of the important points from this result is that the size of Pt crystals can be delicately controlled by tuning the composition of the carbon-carbon composites. When a single carbon support matrix is used, such delicate control of Pt size is not readily achieved.

Figure 7 shows the cyclic voltammetry (CV) results. For the evaluation of fuel cell catalysts, CV measurements mimic the anode reactions of PEM fuel cells. That is, a liquid electrolyte (e.g., H_2SO_4 solution) provides a source of hydrogen to the catalyst. Hydrogen adsorption and desorption processes are represented as the current peaks observed as a function of the voltage sweeps (Figure 7a). The electrochemically active area (ECA, S_{Pt}) measured from the H_2 desorption peaks (the inset of Figure 7a) of the Pt catalysts was calculated using the following equation:

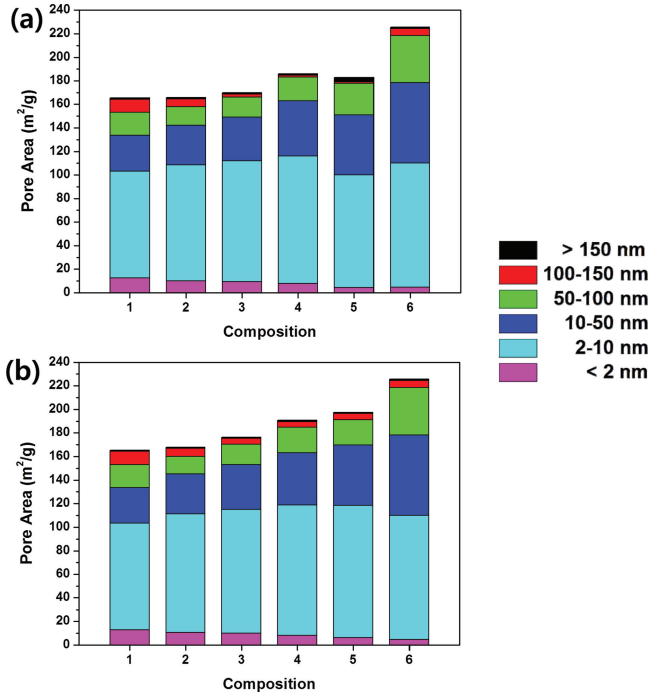

Figure 5. Variation of the pore area of carbon black-nanotube composites as a function of matrix composition (number at bottom of each histogram bar) and pore diameters (see color key). Temperature ramping rate of carbothermal reduction of a) 10 °C/min, and b) 2 °C/min. 1=Vulcan XC72 (CB), 2=CBNT(3:1);), 3=CBNT(2:1), 4=CBNT(1:1), 5=CBNT(1:2), and 6=carbon nanotube (NT).

$$S_{Pt}(m^2/g) = \frac{Q(\mu C/cm^2)}{\{210\,\mu C/cm^2\,Pt \times Pt\ loading\ (mg/cm^2)\} \times 10^4} \quad (2)$$

Here, Q is the charge required for the oxidation of the adsorbed hydrogen on the surface of a Pt electrode, and 210 $\mu C/cm^2$ is the surface charge required for the adsorption and desorption of a monolayer of hydrogen atoms on the surface.[38] The ECA of Pt catalysts synthesized on the different carbon support materials is shown to be inversely proportional (Figure 7b) to the surface area of carbons used as support materials.[17–20] Results of the BET, XRD, and CV measurements are summarized in **Table 2**.

From the results shown in the Figure 6 and Figure 7, an optimal window of the size of Pt nanocrystals required to achieve high electrochemical activity (as determined by CV) is estimated (**Figure 8**). A broad maximum of electrochemical activity centered at about 5–6 nm Pt nanocrystallite size is suggested, although there is some scatter in the data. These results suggest that there is an optimal size range of Pt nanocrystals required to achieve high electrochemical performance, as previously reported by others.[17–20] Control experiments confirm that the synthesis of nanocrystalline Pt achieved by the method described here provides fine control of Pt nanocrystallite size in this range, with uniform nanocrystallite growth and distribution throughout the carbon matrices, in contrast to the larger and more heterogeneous grains formed predominantly on the outer surfaces of the carbon matrices by rapid precipitation methods. Our findings show that kinetically controlled synthesis of the Pt nanocrystals, in conjunction with structural control from the carbon matrix, can be used to tailor the important electrochemical and transport (porosity) properties of the catalytic electrodes for PEM fuel cell applications.

7. Conclusions

A bio-inspired, kinetically controlled synthesis approach was used for the development of a new family of platinum-based fuel cell catalysts. A novel carbon-carbon composite of two different carbon building units, i.e., carbon black and multiwall CNTs, was formed for the control of mesoscale morphology and used as the matrix for nucleation and growth of nanocrystalline Pt. The resulting hierarchical porous structure of Pt@carbon

Table 1. Surface area and pore structure of carbon support materials.

Carbon support[a,b]	Total surface area [m^2/g][c]	Sub-surface area [m^2/g][d]				
		<2 nm	2–10 nm	10–50 nm	50–100 nm	>100 nm
Vulcan XC-72 (CB)	243.20	12.720	90.566	30.372	19.493	12.340
CBNT(3:1)_f	209.31	9.928	98.708	33.519	15.840	7.686
CBNT(2:1)_f	206.85	9.489	102.599	36.849	17.349	3.692
CBNT(1:1)_f	209.23	8.011	108.158	46.852	20.019	2.963
CBNT(1:2)_f	183.30	4.448	95.498	50.908	26.891	4.945
CBNT(3:1)_s	215.28	10.488	100.659	34.052	14.872	7.981
CBNT(2:1)_s	214.32	10.069	105.053	37.972	17.332	5.890
CBNT(1:1)_s	212.32	8.181	110.503	44.653	21.385	6.146
CBNT(1:2)_s	198.82	6.073	112.274	51.317	21.494	6.302
Multi-walled nanotube (NT)	195.22	4.612	105.422	68.185	40.147	7.372

[a]Numbers in parenthesis indicate compositional ratios of carbon black (CB) and nanotube (NT); [b]"f" indicates "fast" (10 °C/min) and "s" indicates "slow" (2 °C/min) ramping rate; [c]total surface area of carbon supports from analyses of BET measurements; [d]surface area in different pore size ranges measured from BJH adsorption.

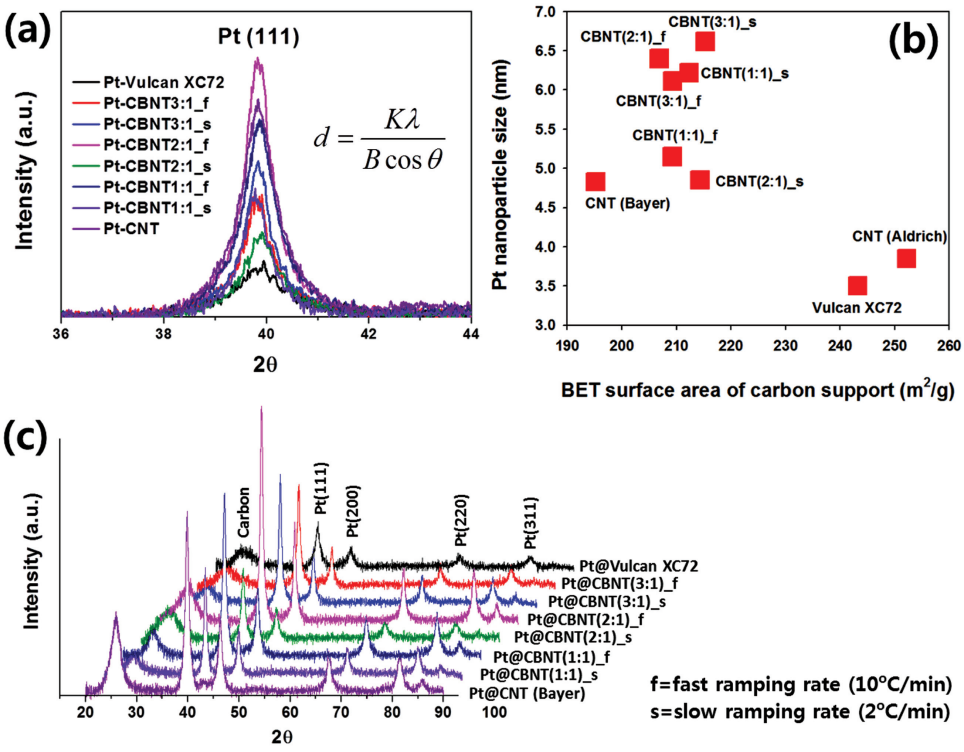

Figure 6. a) XRD peaks of Pt (111) supported on carbon black, CNTs and carbon composites; b) the effect of BET surface area of carbon support matrices on the size of Pt nanocrystals; and c) XRD patterns of Pt@carbon catalysts.

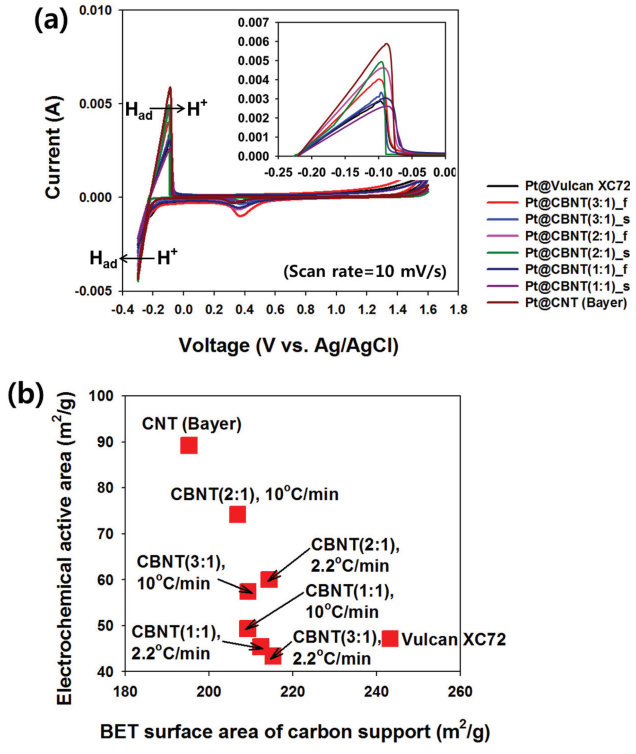

Figure 7. Cyclic voltammograms of Pt catalysts supported on various carbon materials: a) full scanned (scan rate= 10 mV/s) hydrogen adsorption/desorption curves; inset: hydrogen desorption ($H_2 \rightarrow 2H^+ + 2e^-$) current peaks; and b) the relationship between the surface area of carbon support materials and electrochemically active area of catalysts.

Table 2. Relationship between morphology of carbon matrices, Pt nanocrystallite size, and electrochemically active area of 15 wt% Pt@carbon catalysts.

Catalyst	Surface area of carbon [m^2/g][a)]	Pt particle size [nm][b)]	Electrochemical active area [m^2/g][c)]
Pt@Vulcan XC-72	243.20	3.50	47.15
Pt@CNT (Baytube)	195.22	4.83	89.23
Pt@CBNT(1:1)_s	212.32	6.22	45.39
Pt@CBNT(2:1)_s	214.32	4.85	60.03
Pt@CBNT(3:1)_s	215.28	6.62	43.39
Pt@CBNT(1:1)_f	209.23	5.15	49.34
Pt@CBNT(2:1)_f	206.85	6.40	74.17
Pt@CBNT(3:1)_f	209.31	6.11	57.43

[a)]from BET; [b)]from XRD; [c)]from CV.

composite catalysts can be further tailored by tuning the composition and temperature of formation of the carbon-carbon composite. Preliminary voltammetric investigations show that the composite catalyst offers improvement of electrochemical activity over that of the Pt catalysts supported with carbon black (i.e., Vulcan XC-72). These analyses also show an optimal Pt size for highest electrochemical performance, in the range of 5–6 nm, confirming that "smaller is not always better" for electrochemical activity. Our synthesis methods provide access to new combinations of porosity, conductivity and electrochemical hydrogen oxidation. Subsequent studies are required to correlate the properties reported here with performance in PEM fuel cells.

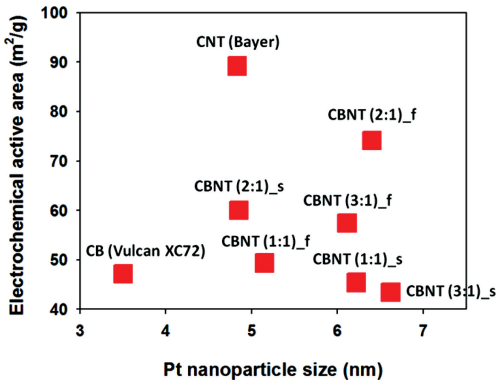

Figure 8. Effect of the size of Pt nanocrystals on the electrochemically active area of Pt@carbon catalysts.

Acknowledgements

This research was supported by the U.S. Department of Energy, Office of Basic Energy Sciences, Division of Materials Sciences and Engineering under Award Grant # DE-FG02-02ER4006. XRD, electron microscopy and other advanced instrumentation were provided by UCSB's Materials Research Laboratory, supported by the MRSEC Program of the National Science Foundation under Award No. DMR 1121053. We thank Bayer Materials Corp. for their gift of multiwall CNTs.

Received: December 31, 2012
Revised: March 21, 2013
Published online: April 30, 2013

[1] D. E. Morse, *Trends Biotechnol.* **1999**, *17*, 230.
[2] J. L. Sumerel, W. Yang, D. Kisailus, J. C. Weaver, J. H. Choi, D. E. Morse, *Chem. Mater.* **2003**, *15*, 4804.
[3] D. Kisailus, J. H. Choi, J. C. Weaver, W. Yang, D. E. Morse, *Adv. Mater.* **2005**, *17*, 314.
[4] S. Litster, G. McLean, *J. Power Sources* **2004**, *130*, 61.
[5] C. S. Kong, D. Y. Kim, H. K. Lee, Y. G. Shul, T. H. Lee, *J. Power Sources* **2002**, *108*, 185.
[6] J. Larminie, A. Dicks, *Fuel Cell Systems Explained*, John Wiley & Sons, Inc., Baffins Lane, UK **2000**.
[7] E. Antolini, *J. Mater. Sci.* **2003**, *38*, 2995.
[8] C. Coutanceau, S. Baranton, T. W. Napporn, in *The Delivery of Nanoparticles* (Ed: A. A. Hashim), InTech **2012**, Ch. 19.
[9] K. Kinoshita, *Carbon: Electrochemical and Physicochemical Properties*, John Wiley & Sons, New York **1988**.
[10] P. J. F. Harris, in *Chemistry and Physics of Carbon*, *vol. 28* (Ed: L. R. Radovic), Marcel Dekker, New York **2003**, Ch. 1.
[11] N. Job, S. Berthon-Fabry, M. Chatenet, J. Marie, M. Brigaudet, J.-P. Pirard, *Top. Catal.* **2009**, *52*, 2117.
[12] S. Song, Y. Liang, Z. Li, Y. Wang, R. Fu, D. Wu, P. Tsiakaras, *Appl. Cat. B* **2010**, *98*, 132.
[13] G. Wu, Y.-S. Chen, B.-Q. Xu, *Electrochem. Commun.* **2005**, *7*, 1237.
[14] K. A. Mauritz, *JMS-Rev. Macromol. Chem. Phys.* **1988**, *C28*, 65.
[15] M. Uchida, Y. Aoyama, N. Eda, A. Ohta, *J. Electrochem. Soc.* **1995**, *142*, 4143.
[16] M. Uchida, Y. Fukuoka, Y. Sugawara, N. Eda, A. Ohta, *J. Electrochem. Soc.* **1996**, *143*, 2245.
[17] M. Uchida, Y. Fukuoka, Y. Sugawara, H. Ohara, A. Ohta, *J. Electrochem. Soc.* **1998**, *145*, 3708.
[18] Z. Xie, T. Navessin, X. Zhao, M. Adachi, S. Holdcroft, T. Mashio, A. Ohma, K. Shinohara, *ECS Trans.* **2008**, *16*, 1811.
[19] M. Watanabe, H. Sei, P. Stonehart, *J. Electroanal. Chem.* **1989**, *261*, 375.
[20] K. Kinoshita, *J. Electrochem. Soc.* **1990**, *137*, 845.
[21] K. Yahikozawa, Y. Fujii, Y. Matsuda, K. Nishimura, Y. Takasu, *Electrochim. Acta* **1991**, *36*, 973.
[22] A. Kabbabi, F. Gloaguen, F. Andolfatto, R. Durand, *J. Electroanal. Chem.* **1994**, *373*, 251.
[23] S. Mann, *Biomineralization: Principles and Concepts in Bioinorganic Materials Chemistry*, Oxford University Press, Oxford, UK **2001**.
[24] S. Mann, *Biomimetic Materials Chemistry*, VCH, New York **1996**.
[25] B. Schwenzer, K. M. Roth, J. R. Gomm, M. Murr, D. E. Morse, *J. Mater. Chem.* **2006**, *16*, 401.
[26] D. Kisailus, B. Schwenzer, J. Gomm, *J. Am. Chem. Soc.* **2006**, *128*, 10276.
[27] R. L. Brutchey, D. E. Morse, *Chem. Rev.* **2008**, *108*, 4915.
[28] H.-L. Zhang, D. E. Morse, *J. Mater. Chem.* **2009**, *19*, 9006.
[29] T. Ould-Ely, M. Luger, L. Kaplan-Reinig, K. Niesz, M. Doherty, D. E. Morse, *Nat. Protoc.* **2011**, *6*, 97.
[30] J. E. Sheehan, K. W. Buesking, B. J. Sullivan, *Annu. Rev. Mater. Sci.* **1994**, *24*, 19.
[31] Y. Li, Y. Li, E. Zhu, T. McLouth, C.-Y. Chiu, X. Huang, Y. Huang, *J. Am. Chem. Soc.* **2012**, *134*, 12326.
[32] X. L. Wang, H. M. Zhang, J. L. Zhang, H. F. Xu, Z. Q. Tian, J. Chen, H. X. Zhong, Y. M. Liang, B. L. Yi, *Electrochim. Acta* **2006**, *51*, 4909.
[33] M. M. Shaijumon, S. Ramaprabhu, N. Rajalakshmi, *Appl. Phys. Lett.* **2006**, *88*, 253105.
[34] Y. S. Yun, D. Kim, Y. Tak, H.-J. Jin, *Synth. Met.* **2011**, *161*, 2460.
[35] E. Bekyarova, M. E. Itkis, N. Cabrera, B. Zhao, A. Yu, J. Gao, R. C. Haddon, *J. Am. Chem. Soc.* **2005**, *127*, 5990.
[36] J. I. Langford, A. J. C. Wilson, *J. Appl. Cryst.* **1978**, *11*, 102.
[37] K. S. W. Sing, D. H. Everett, R. A. W. Haul, L. Moscou, R. A. Pierotti, J. Rouquerol, T. Siemieniewska, *Pure Appl. Chem.* **1985**, *57*, 603.
[38] A. Pozio, M. D. Francesco, A. Cemmi, F. Cardellini, L. Giorgi, *J. Power Sources* **2002**, *105*, 13.